

# LANL Report LA-UR-99-360 (1999)

Submitted to *Nucl. Instr. Meth. A* and to be presented at the *American Physical Society Centennial Meeting, Atlanta, Georgia, March 20-26, 1999*

## Computer Study of Isotope Production in High Power Accelerators

K. A. Van Riper<sup>a</sup>, S. G. Mashnik<sup>b</sup>, and W. B. Wilson<sup>b</sup>

<sup>a</sup> *White Rock Science, PO Box 4729, Los Alamos, NM 87544*

<sup>b</sup> *T-2, Theoretical Division, Los Alamos National Laboratory, Los Alamos, NM 87545*

### Abstract

Methods for radionuclide production calculation in a high power proton accelerator have been developed and applied to study production of 22 isotopes by high-energy protons and neutrons. These methods are readily applicable to accelerator, and reactor, environments other than the particular model we considered and to the production of other radioactive and stable isotopes. We have also developed methods for evaluating cross sections from a wide variety of sources into a single cross section set and have produced an evaluated library covering about a third of all natural elements. These methods also are applicable to an expanded set of reactions. A 684 page detailed report on this study, with 37 tables and 264 color figures is available on the Web at <http://t2.lanl.gov/publications/publications.html>, or, if not accessible, in hard copy from the authors.

### 1. Introduction

The widespread use of radionuclides in medical and industrial applications is steadily increasing, leading suppliers to seek out new production facilities. A reliable supply chain is necessary to both encourage new applications and to replace aging production sources. The United States, in particular, faces a domestic production shortfall. It has been a policy of this country to import radioisotopes from Canada and other countries. The lack of a reliable supply has led to supply problems at times that could be ameliorated by a domestic production facility.

Among the possibilities for radionuclide production are high power accelerators, either purpose built or alongside existing applications. As an example of the latter, a recent study by the Medical University of South Carolina [1] discussed the production of medical radioisotopes at the proposed Accelerator Production of Tritium Facility (APT) [2]. For instance, the comprehensive report [1] states: “The Committee on Biomedical Isotopes (Institute of Medicine) concluded that a dedicated facility, such as the proposed National Biomedical Facility (NBTF) which was a focus of their report, is not economically justified as a source of radionuclides, whether such a facility were a reactor or an accelerator [3]. However, nuclides produced at a facility in operation primarily for other purposes would incur only incremental costs and therefore be a more cost effective means of production; contributions from the revenue stream of radionuclide sales would partially, if not completely, offset the incurred incremental costs of production.” The report [1] considered a large number of radioisotopes for present or future applications in medical treatment and diagnostic procedures. Many of these radioisotopes could

be produced in the intense and energetic neutron and proton fluxes characteristic of the APT target and blanket assembly.

We have undertaken a study to see to what extent existing nuclear data models are applicable to calculations of radionuclide production in a high energy, high power environment. We chose the APT target/blanket assembly as a typical environment in which to study isotope production. In addition to the availability of existing input models for our Monte Carlo flux calculations, the high energies of the neutron and proton fluxes offer a formidable test of the nuclear data. In a previous report [4], we considered the production of two radioisotopes –  $^{18}\text{F}$  and  $^{131}\text{I}$  – at two locations in the APT blanket. We have extended that study to look at the production rates of 22 isotopes in nearly 500 locations throughout the APT target and blanket. In addition to the 100 milliamp 1.7 GeV proton beam energy assumed in the previous study, we also treat beam energies of 1.0, 1.2, 1.4, 1.6, and 1.8 GeV (all at 100 milliamps).

It should be noted that we have chosen the APT accelerator for our study as an example with which to demonstrate the possibility of production of radioisotopes at such a facility. Radioisotopes can be produced also at other high power accelerators, projected for the accelerator transmutation of nuclear wastes (ATW) or other needs, such as the new spallation sources under consideration in USA, Europe, Japan and elsewhere [5]-[8], as well as at different nuclear reactors. Our computational method is not limited to a particular facility and can be used to study production of radioactive as well as stable isotopes at any accelerator or reactor. For practical reasons, the emphasis of our present study is on radioisotopes.

The production rate of a radioisotope can be obtained from the integral of the flux and cross section leading to the direct production of the radioisotope as a reaction product. Additional production is realized from other radionuclides that decay to the desired product. Evaluation of production rates then requires knowledge of the neutron and proton fluxes at some position in the production facility and cross sections leading to production of the desired radionuclide and its progenitors. Ideally, one would use a cross section library that includes data for all nuclides in the neighborhood of the desired product in a transmutation code. Construction of such a comprehensive library is beyond the scope of the present study. Instead, we evaluated cross sections for reactions most likely to lead to our desired products [9].

We have prepared numerous figures and tables as part of this work. Space available in this paper prevents their inclusion here. Our 684 page detailed report on this study [10], with 37 tables and 264 color figures is available on the World Wide Web under:

<http://t2.lanl.gov/publications/publications.html>. We will provide also a link to exact location in:

[http://www.rt66.com/~kvr/kvr\\_pubs.html#CONTRIBUTED](http://www.rt66.com/~kvr/kvr_pubs.html#CONTRIBUTED), and a limited number of hard copies may be available from the authors.

## 2. APT Modeling and Flux Tallies

Figure 1 is a 3-dimensional rendering of a computer model of the target/blanket assembly. The model is based on the Todosow geometry with a 16 cm  $\times$  160 cm beam area. The beam enters the assembly through the green window on the right. The beam strikes tungsten-dominated ladders in the center of the assembly; the position of these ladders correspond to the pipes extending from the yellow manifolds. The lateral blankets extend to either side of the beam line and ladder area. The downstream blanket encompasses the region to the left of the ladder region, while the upstream blanket is the narrow area between the entrance window and the ladder region.

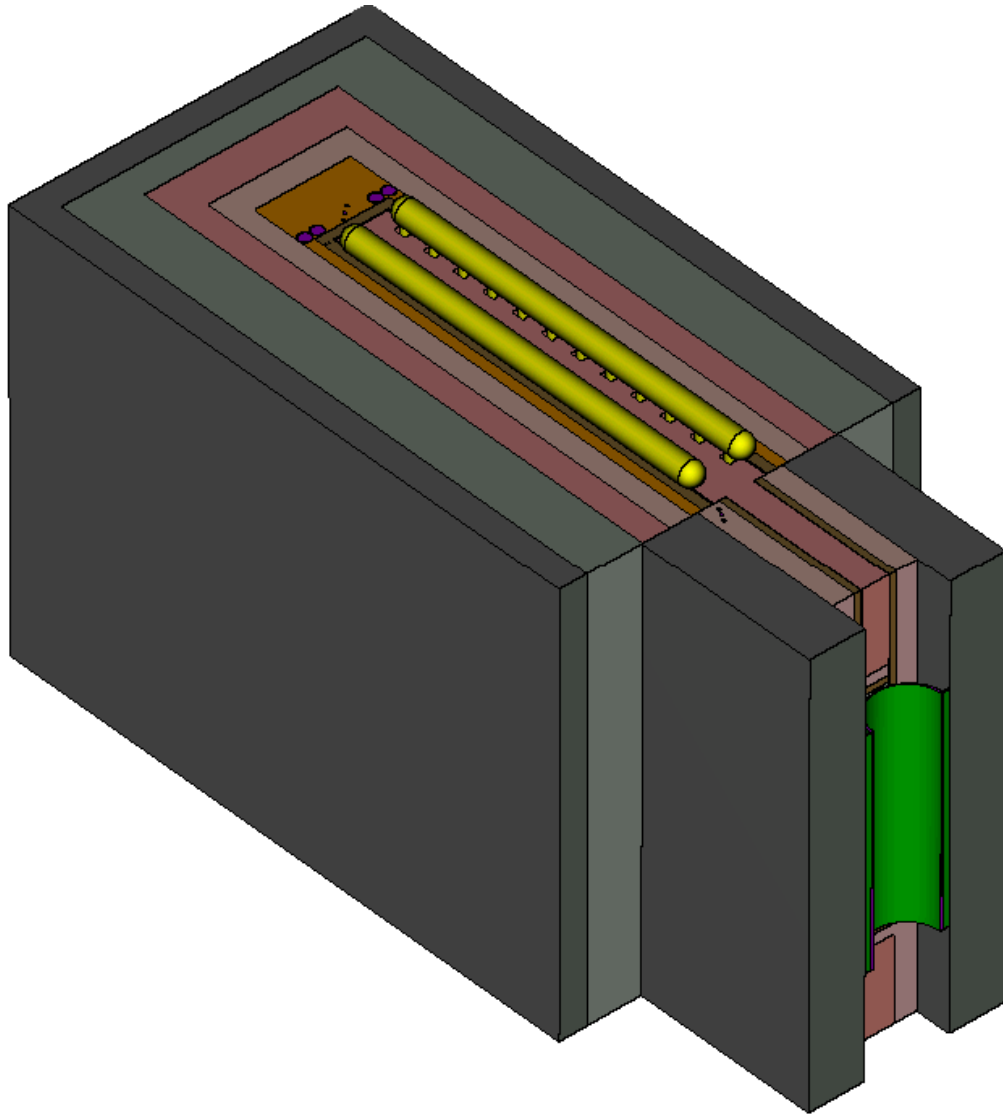


Fig. 1. APT target/blanket assembly.

We used MCNPX version 2.1.1 to calculate neutron and proton fluxes throughout the APT model, excluding pipes and ladders within the beam cavity and some regions at the bottom of the model. We made runs for beam energies of 1.0, 1.2, 1.4, 1.6, 1.7, and 1.8 GeV, assuming a 100 milliamp beam in each case. For each case, the runs followed 120,000 incident protons.

**Tally Locations.** Subdivision of cells in the upstream, downstream, and lateral blanket regions and in the beam cavity between ladders yielded approximately 183 cells in which the fluxes were tallied. Figure 2 shows the cell locations in a slice in the X-Z plane through the middle of the target model. We did not tally fluxes in the ladders (red areas in Figure 1), nor in the coolant pipes (green areas).

Assuming reflective symmetry in the X direction (where Z is the beam direction and Y is the vertical direction), tallies were taken over the union of a cell on the -X side of the beam with its +X counterpart. Three such pairs of symmetric cells are shaded light gray, yellow, and light blue in Figure 2. Accounting for cells symmetric about  $X = 0$ , there were 102 tallies.

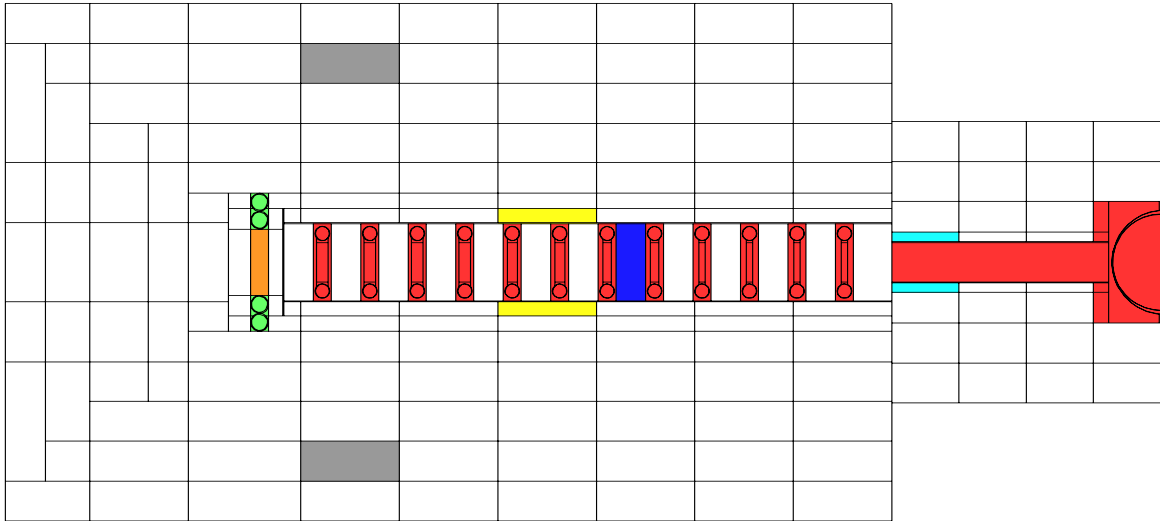


Fig. 2. A slice through the middle of the APT target/blanket assembly showing cells where tallies were taken.

**Vertical Segments.** We segmented the tallies into five equally spaced vertical segments. Figure 3, a cross section through the upstream blanket, shows the segmenting. Segment 1 is the topmost segment, Segment 3 is in the middle position, and Segment 5 is the lowest. With a few exceptions, all cells in the blankets extend the full height of the target, while the cells in the beam line do not extend to the topmost and lowest segments. The fluxes, and hence production rates, were greatest in the middle segment (3), decreasing towards the top and bottom. Unless otherwise stated, the results presented here are for the middle segment.

**Locations for Detailed Results.** We present detailed summaries of the production rates at four locations. Two of these locations, in the upstream (light blue cells in Fig. 2) and downstream (orange cell) blankets, were chosen to overlap the locations used in the previous study. The other two locations, one behind the fifth ladder in the beam cavity (dark blue cell in Fig. 2) and the other opposite the sixth, seventh, and eighth ladders in the first lateral blanket row (yellow cells), are the locations of maximum production rates for a great majority of reactions. For each reaction, we found the cell with the maximum rate over our entire set of tallies, and the cell with the maximum rate over all tallies excluding the beam cavity cells. In approximately 80% of the reactions, this procedure picked our two selected locations. For all but a handful of the remaining reactions, the picked cells were a neighbor of the selected locations.

We did not model any fixtures, such as irradiation tubes, that would be required to produce radioisotopes in any location. Our results thus assume any such fixtures would have no effect on the fluxes.

Spectrum plots of the neutron and proton fluxes in each segment of the four selected locations are given in our detailed report available on the Web [10].

**Flux Color Contours on Planes.** We prepared a variation of the target geometry for display of the fluxes (and production rates) as color-coded contours on a plane. We introduced

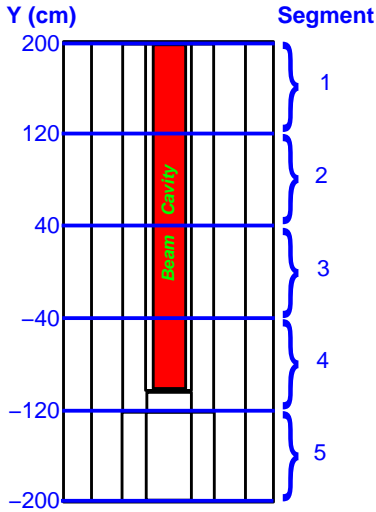


Fig. 3. A cross section through the upstream section of the APT target/blanket assembly showing the vertical segment used in the tallies.

5 planes to represent the 5 vertical segments; the vertical position of the plane lies at the center of the corresponding segment. Each plane thus represents the flux averaged over a segment. For visual orientation, we included the ladders, top manifolds, and other elements in the revised geometry; these elements, shown in gray in the plots, represent cells in which we did not take a flux tally. (This revised model is used for visualization only; it was not used in the flux calculations.)

Figure 4 shows a color contour plot of the neutron flux for a 1.0 GeV beam energy. The detailed Web report [10] includes similar plots for neutron and proton flux contours at the 6 energies we consider.

### 3. Cross Section Evaluations

Our earlier work [4] involved the modeling of neutron- and proton-induced reactions on isotopes of O, F, Ne, Na, Mg, Al, Xe, Cs, Ba and La for energies to 1.7 GeV. We have now added reactions on isotopes of S, Cl, Ar, K, Zn, Ga, Ge, As, Zr, Nb, Mo and Hg.

At present, neither available experimental data nor any of the current models or phenomenological systematics can be used alone to produce a reliable evaluated activation cross section library covering a large range of target nuclides and incident energies. Therefore, we chose to create our evaluated library [9] by constructing excitation functions using all available experimental data along with calculations using some of the more reliable codes, employing each of these sources in the regions of targets and incident energies where they are most applicable. When we have reliable experimental data, they, rather than model results, are taken as the highest priority for our approximation. Wherever possible, we attempted to construct a smooth transition from one data source to another.

The recent *International Code Comparisons for Intermediate Energy Nuclear Data* organized by NEA/OECD at Paris [11], our own comprehensive benchmarks [4, 9, 10, 12, 13], and several studies by Titarenko et al. [14] have shown that a modified version of the Cascade-Exciton model (CEM) [15] as realized in the code CEM95 [16] and LAHET code system [17, 18] generally have the best predictive powers for spallation reactions at energies above 100 MeV as compared to other available models.

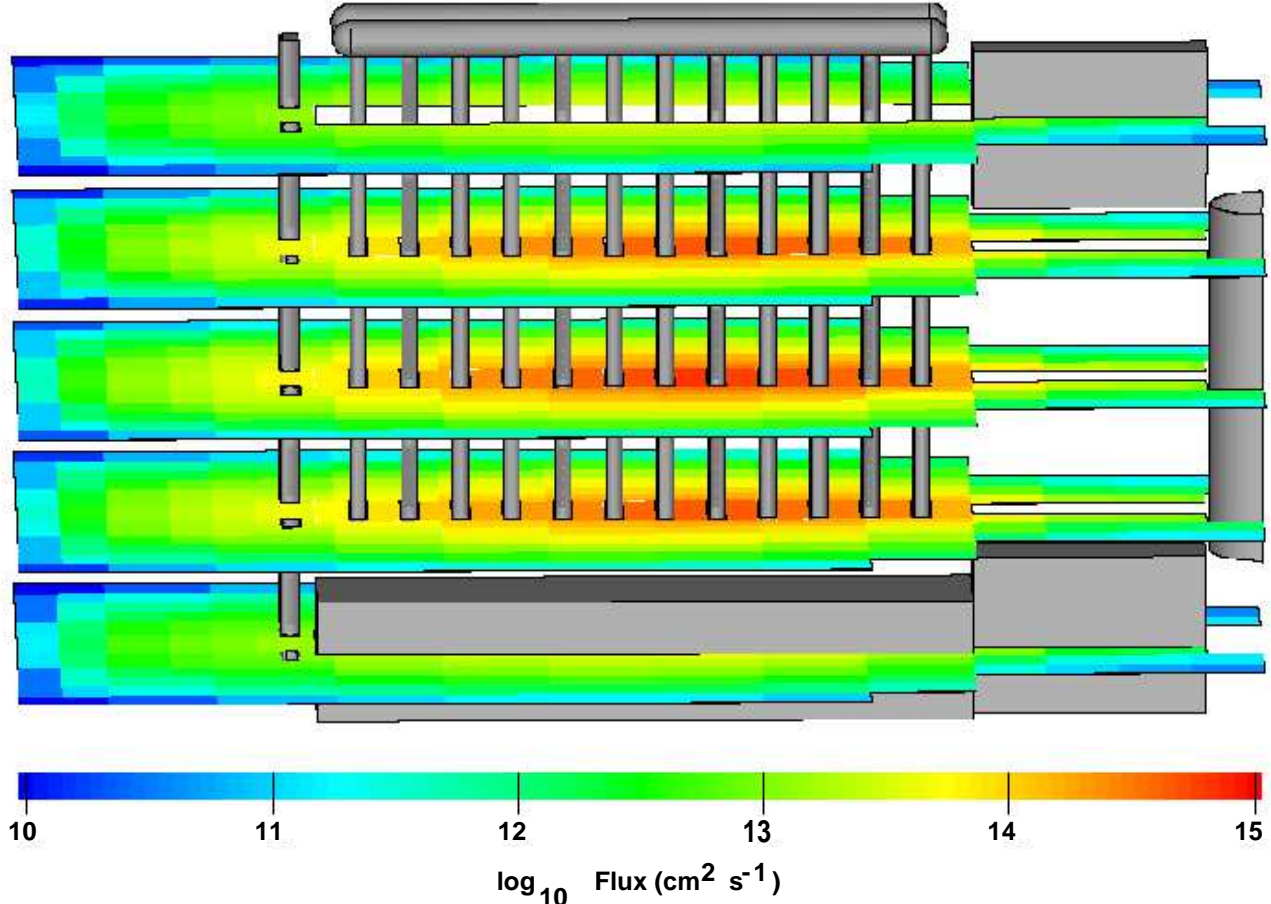


Fig. 4. Color contours of the neutron flux at a beam energy of 1.0 GeV.

Therefore, we choose CEM95 [16], the recently improved version of the CEM code [19], and LAHET (version 2.83) [17, 18] above 100 MeV to evaluate the required cross sections. Specifically, we employ the calculated library described in [9]. The same benchmarks have shown that at lower energies, the HMS-ALICE code [20] most accurately reproduces experimental results as compared with other models. We therefore use the activation library calculated by M. B. Chadwick [21] with the HMS-ALICE code [20] for protons below 100 MeV and neutrons between 20 and 100 MeV. In the overlapping region, between 100 and 150 MeV, we use both HMS-ALICE and CEM95 and/or LAHET results. For neutrons below 20 MeV, we consider the data of the European Activation File EAF-97, Rev. 1 [22, 23] with some recent improvements by M. Herman [24], to be the most accurate results available; therefore we use them as the first priority in our evaluation.

Measured cross-section data from our compilation described in [9], when available, are included together with theoretical results and are used to evaluate cross sections for study. We note that when we put together all these different theoretical results and experimental data, rarely do they agree perfectly with each other, providing a smooth continuity of evaluated excitation functions. Often, the resulting compilations show significant disagreement at energies where the available data progresses from one source to another. These sets are thinned to eliminate discrepant data, providing data sets of more-or-less reasonable continuity defining our evaluated cross sections [9] used here.

Examples with typical results of evaluated activation cross sections for several proton reactions are shown in Fig. 5. by broad gray lines. 51 similar color figures for proton-induced reactions and 57 figures for neutrons, can be found on the Web, in our detailed report [10].

Our cross section tables reach to a maximum energy of 1.7 GeV. Between 1.7 and 1.8 GeV, we used the value at 1.7 GeV. Because most cross sections are relatively independent of energy at these high energies, this assumption should not be far removed from reality.

## 4. Production Rate Calculations

We consider production rates for the following 22 end product nuclides of medical importance [1]:

$^{18}\text{F}$	$^{35}\text{S}$	$^{89}\text{Sr}$	$^{133}\text{Xe}$
$^{22}\text{Na}$	$^{67}\text{Cu}$	$^{89}\text{Zr}$	$^{131}\text{Cs}$
$^{32}\text{Si} / ^{32}\text{P}$	$^{67}\text{Ga}$	$^{95}\text{Zr}$	$^{137}\text{Cs}$
$^{32}\text{P}$	$^{68}\text{Ga}$	$^{95}\text{Nb}$	$^{193m}\text{Pt}$
$^{33}\text{P}$	$^{68}\text{Ge} / ^{68}\text{Ga}$	$^{131}\text{I}$	$^{195m}\text{Pt}$

To produce these nuclides, we calculated neutron and proton reactions on the stable, naturally occurring isotopes of elements in the neighborhood of the targets investigated. These 70 nuclides of 25 elements are:

$^{18}\text{O}$	$^{32}\text{S}$	$^{66}\text{Zn}$	$^{89}\text{Y}$	$^{130}\text{Xe}$	$^{193}\text{Ir}$
	$^{33}\text{S}$	$^{67}\text{Zn}$		$^{131}\text{Xe}$	
$^{19}\text{F}$	$^{34}\text{S}$	$^{68}\text{Zn}$	$^{90}\text{Zr}$	$^{132}\text{Xe}$	$^{197}\text{Au}$
	$^{36}\text{S}$	$^{70}\text{Zn}$	$^{91}\text{Zr}$	$^{134}\text{Xe}$	
$^{20}\text{Ne}$		$^{92}\text{Zr}$		$^{136}\text{Xe}$	$^{196}\text{Hg}$
$^{21}\text{Ne}$	$^{35}\text{Cl}$	$^{69}\text{Ga}$	$^{94}\text{Zr}$		$^{198}\text{Hg}$
$^{22}\text{Ne}$	$^{37}\text{Cl}$	$^{71}\text{Ga}$	$^{96}\text{Zr}$	$^{133}\text{Cs}$	$^{199}\text{Hg}$
					$^{200}\text{Hg}$
$^{23}\text{Na}$	$^{36}\text{Ar}$	$^{70}\text{Ge}$	$^{93}\text{Nb}$	$^{134}\text{Ba}$	$^{201}\text{Hg}$
	$^{38}\text{Ar}$	$^{72}\text{Ge}$		$^{135}\text{Ba}$	$^{202}\text{Hg}$
$^{24}\text{Mg}$	$^{40}\text{Ar}$	$^{73}\text{Ge}$	$^{92}\text{Mo}$	$^{136}\text{Ba}$	$^{204}\text{Hg}$
$^{25}\text{Mg}$		$^{74}\text{Ge}$	$^{94}\text{Mo}$	$^{137}\text{Ba}$	
$^{26}\text{Mg}$	$^{39}\text{K}$	$^{76}\text{Ge}$	$^{95}\text{Mo}$	$^{138}\text{Ba}$	
	$^{40}\text{K}$		$^{96}\text{Mo}$		
	$^{41}\text{K}$		$^{97}\text{Mo}$	$^{138}\text{La}$	
$^{27}\text{Al}$		$^{75}\text{As}$	$^{98}\text{Mo}$	$^{139}\text{La}$	
			$^{100}\text{Mo}$		

For each reaction, we

- 1) constructed a continuous energy representation of the cross section from the evaluation tables;
- 2) formed a flux-weighted average cross section for each particle flux at each location;
- 3) computed the one-hour irradiation end product  $P$  production rate per gram of target to each target nuclide / reaction product  $p$  radionuclide combination;
- 4) formed the one hour irradiation production rate per gram of target nuclide or naturally occurring element.

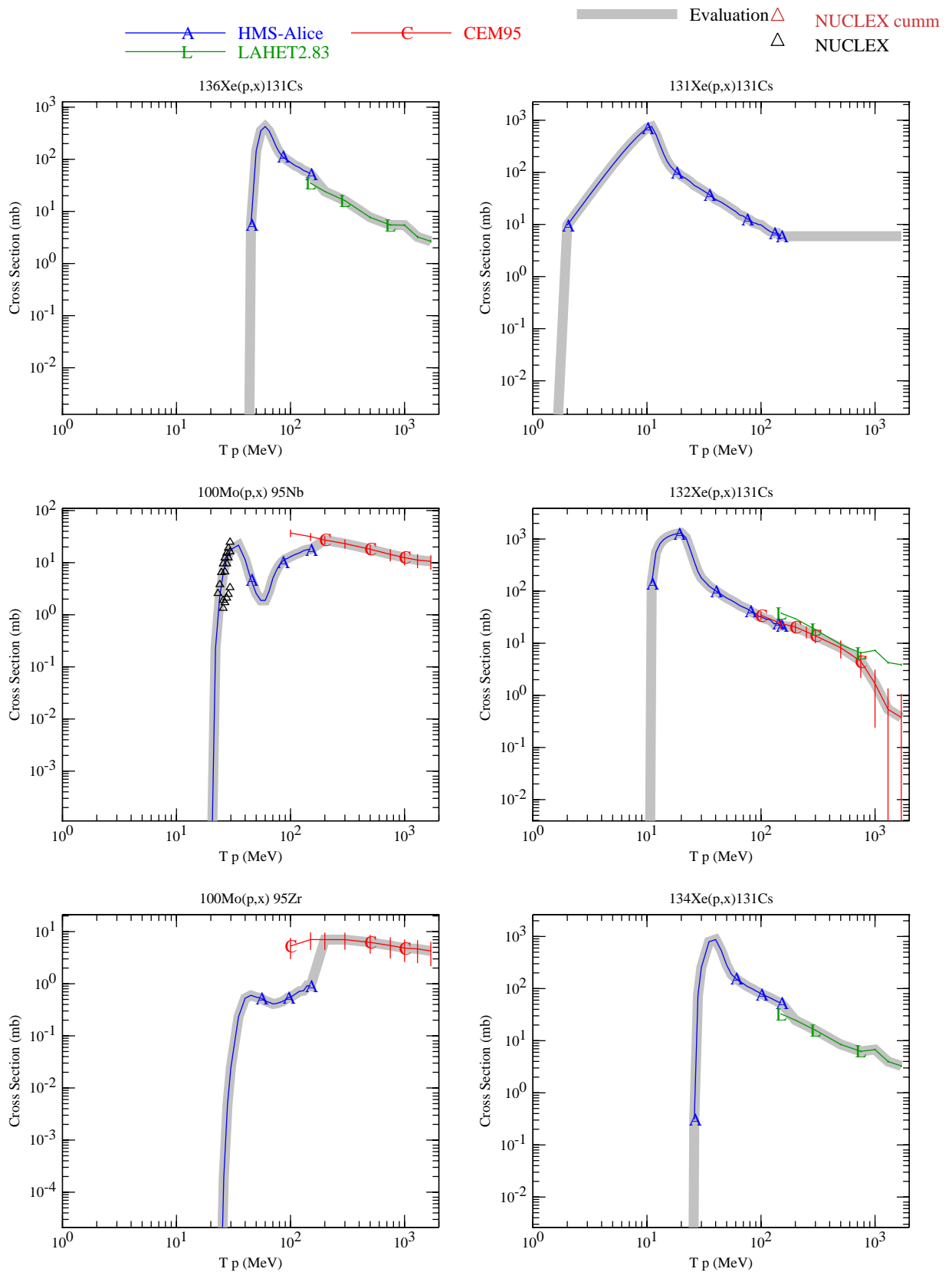


Fig. 5. Examples of several evaluated proton-induced activation cross sections. Evaluated cross sections are shown by broad gray lines, other notations are given in the plots and described in the text and in [9].



The flux-weighted cross section  $\sigma_{tp}$  for each target  $t$  and reaction product  $p$  is found by

$$\sigma_{tp} = \frac{\int_0^\infty \phi(E)\sigma_{tp}(E)dE}{\int_0^\infty \phi(E)dE} = \frac{\sigma_{tp}\Phi}{\Phi} .$$

The cross section  $\sigma_{tP}$  leading to end product  $P$  is taken as the sum of all cross sections for the direct production of  $P$  and products  $p$  decaying to  $P$ . The cross section  $\sigma_{ZP}$  for element  $Z$  leading to end product  $P$  is obtained as the natural-abundance-weighted sum of the cross sections  $\sigma_{tP}$  of the various naturally occurring target nuclides of the element. For intermediate nuclides that have multiple decay paths, we multiply the rate to account for the branching factors to the desired end product.

The production rate  $R_{tP}$  (Ci/g-hr) for each target  $t$  – end product  $P$  combination is

$$R_{tP} = N_t\sigma_{tP}\Phi[1 - \exp(-\lambda_p T)] ,$$

where  $\lambda_p$  is the decay constant ( $s^{-1}$ ) of end product  $P$ ,  $T = 3600s$  corresponds to a one-hour irradiation,  $N_t = N_0/A_t$  is the atom density (atoms/g) of the target material,  $N_0$  is Avogadro's number ( $6.022 \times 10^{23}$  atoms/mole), and  $A_t$  is the atomic weight of the target.  $A_t$  is taken as the integer mass number for isotopic targets and as the atomic weight for the elements.

## 5. Isotope Production Rates

As an example, Table 1 shows a small part of our final results, for the production rates of only  $^{18}\text{F}$ , for the upstream and downstream blanket positions for a 1.7 GeV beam energy. This is just to have an idea how look our complete tables in our Web report [10] for the production all isotopes studied. The Web version of the report includes similar but complete tables for other beam energies. Also, on the Web are tables that gives detail of these production rates, including the flux-averaged cross sections and production rates for intermediate products, and color contour plots of production rates for natural element target at a beam energy of 1.7 GeV.

Table 1  
Production Rates in Forward and Downstream Blanket Locations for a 1.7 GeV Beam Energy

Target Nuclide	Product Nuclide	Forward Blanket			Downstream Blanket		
		Protons Ci/g-hr	Neutrons Ci/g-hr	Total Ci/g-hr	Protons Ci/g-hr	Neutrons Ci/g-hr	Total Ci/g-hr
<i>nat</i> O	$^{18}\text{F}$	2.87E-06	0.00E+00	2.87E-06	1.66E-05	0.00E+00	1.66E-05
<i>nat</i> F	$^{18}\text{F}$	7.96E-03	7.69E-02	8.48E-02	7.73E-02	2.23E-01	3.00E-01
$^{20}\text{Ne}$	$^{18}\text{F}$	5.16E-03	1.29E-02	1.81E-02	5.35E-02	7.85E-02	1.32E-01
$^{21}\text{Ne}$	$^{18}\text{F}$	2.91E-03	3.52E-03	6.44E-03	2.99E-02	2.86E-02	5.85E-02
$^{22}\text{Ne}$	$^{18}\text{F}$	2.47E-03	1.52E-03	3.99E-03	2.20E-02	1.45E-02	3.65E-02
<i>nat</i> Ne	$^{18}\text{F}$	4.89E-03	1.17E-02	1.66E-02	5.03E-02	7.20E-02	1.22E-01
<i>nat</i> Na	$^{18}\text{F}$	2.43E-03	1.02E-02	1.27E-02	2.41E-02	5.11E-02	7.52E-02
$^{24}\text{Mg}$	$^{18}\text{F}$	2.04E-03	4.29E-03	6.33E-03	2.21E-02	2.87E-02	5.08E-02
$^{25}\text{Mg}$	$^{18}\text{F}$	1.48E-03	1.95E-03	3.43E-03	1.68E-02	1.57E-02	3.24E-02
$^{26}\text{Mg}$	$^{18}\text{F}$	1.14E-03	9.73E-04	2.11E-03	1.26E-02	9.30E-03	2.19E-02
<i>nat</i> Mg	$^{18}\text{F}$	1.88E-03	3.66E-03	5.54E-03	2.04E-02	2.51E-02	4.55E-02
<i>nat</i> Al	$^{18}\text{F}$	1.15E-03	1.16E-03	2.31E-03	1.32E-02	9.67E-03	2.28E-02

## 6. Dependence on Position and Beam Energy

We selected three groups of cells, all in the middle segment, to explore the dependence of the production rates on position in the target/blanket assembly and on the beam energy. Figure 6, a slice in the X-Z plane through the middle of the target, shows the groupings. The *Beam Cavity Cells* are light blue, the *Downstream Cells* are dark blue, and the *Lateral Cells* are yellow. The orange cell belongs to both the cavity and lateral groups.

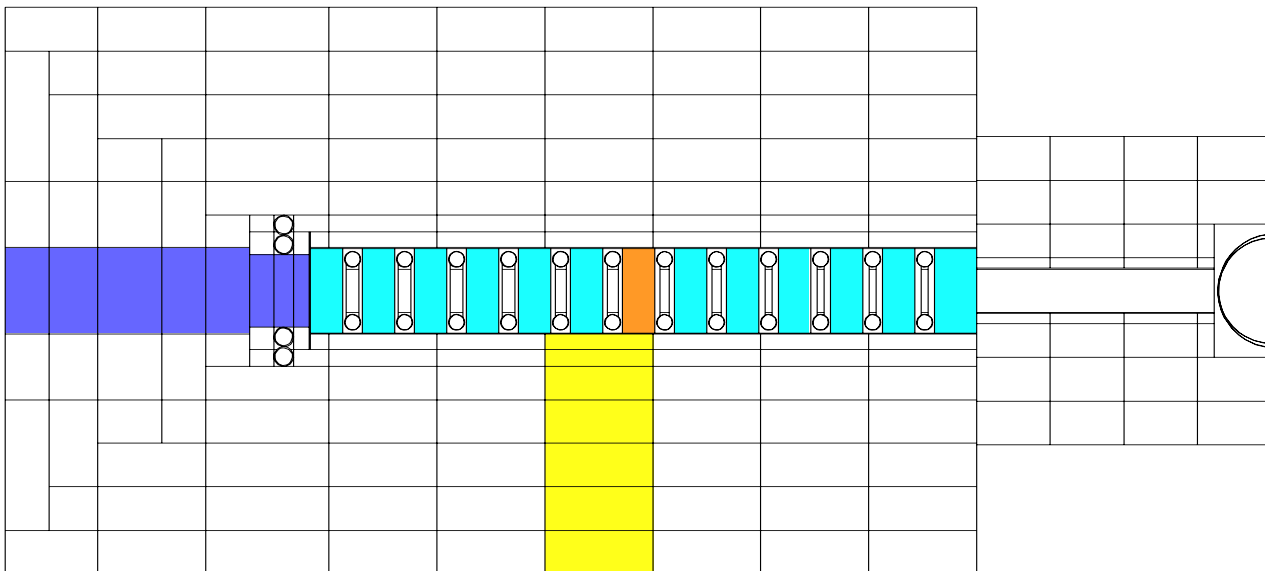


Fig. 6. A slice through the middle of the APT target/blanket assembly showing the locations of the cell grouping in the energy and distance dependence studies.

For the beam cavity cells, the distance is measured along the beam starting at the first upstream light blue cell. For the downstream cells, the distance is measured from the end of the beam cavity. The lateral distance is from the centerline of the beam cavity towards the outside of the assembly.

Figures showing the variation of production rates with beam energy and distance from natural element targets are included in the Web version of the report. The rates increase with beam energy, by between factors of 1.5 and 5 from beam energies of 1.0 to 1.8 GeV. The downstream cells closest to the beam cavity are less sensitive to beam energy than those further downstream. There is less spread in the beam energy dependence in the lateral cells than in the other groups. Within the beam cavity, the rates peak at a distance of 140 cm. The rates decrease exponentially with distance into the lateral blanket. Downstream of the first few cells in the downstream blanket, the rates also decrease exponentially with distance into the downstream blanket.

## 7. Summary

We have characterized the radiation environment in a high power proton accelerator and developed methods for radionuclide production calculations. These methods are readily applicable to accelerator, and reactor, environments other than the particular model we considered and to the production of other radioactive and stable isotopes. We have also developed methods for evaluation cross sections from a wide variety of sources into a single cross section set. These methods also are applicable to an expanded set of reactions.

While the agreement among the different cross section models and with experimental data is good for quite a few reactions, a significant number of reactions remain problematical. A particular problem is the lack of high energy data for  $^{193m}\text{Pt}$  and  $^{195m}\text{Pt}$  production. We will look into the possibility of extracting excited state production from LAHET and other calculations in future work.

Commenting on the feasibility and economic viability of the production of any particular isotope is beyond the scope of this work. Such information, which must come from experts in the radionuclide arena, will be a vital ingredient in choosing which cross sections should be subjected to greater scrutiny.

This study of isotope production in targets within an accelerator spallation target/blanket assembly is particular to the APT — now the backup concept for tritium production in the US DOE. Because of the broad range of beam energy and target positioning in the study, as well as the spatial mapping of neutron and proton fluxes and isotope production throughout the geometry, results are applicable to a wide range of beam energies and beam intensities of spallation targets now under consideration in the USA, Europe, Japan and elsewhere.

## Acknowledgements

We thank many colleagues, in particular M. B. Chadwick and A. J. Sierk, for fruitful collaboration with us at different stages of this work. We express our gratitude to R. E. MacFarlane and L. S. Waters for interest in and support of the present work. This study was partially supported by the U. S. Department of Energy.

## References

- [1] K. M. Spicer, S. Baron, G. D. Frey, G. Blanpied, D. Adcock, S. E. Davis, J. R. Frysenger, and D. C. McLean, Jr., "Evaluation of Medical Radionuclide Production with the Accelerator Production of Tritium (APT) Facility," Medical University of South Carolina final report (July 15, 1997).
- [2] J. C. Browne, J. L. Anderson, M. W. Cappiello, G. P. Lawrence, and P. W. Lisowski, "Status of the Accelerator Production of Tritium (APT) Project," Proc. APT Symp. *The Savannah River Accelerator Project and Complementary Spallation Neutron Sources*, University of South Carolina, Columbia, USA, May 14-15, 1996, F. T. Avignone and T. A. Gabriel, eds., World Scientific, Singapore, 1998, p. 14.
- [3] S. J. Adelstein, *Isotopes for Medicine and Life Sciences*, F. J. Manning, eds., Washington, D.C.: National Academy Press, (1995).

- [4] K. A. Van Riper, S. G. Mashnik, M. B. Chadwick, M. Herman, A. J. Koning, E. J. Pitcher, A. J. Sierk, G. J. Van Tuyle, L. S. Waters, and W. B. Wilson, “APT Medical Isotope Production Study:  $^{18}\text{F}$  and  $^{131}\text{I}$  Production,” Los Alamos Report LA-UR-97-5068 (1997); [hppt://t2.lanl.gov/publications/publications.html](http://t2.lanl.gov/publications/publications.html).
- [5] W. Gudowski, Proc. Int. Workshop on Nucl. Methods for Transmutation of Nuclear Wastes: Problems, Perspectives, Cooperative Research, Dubna, Russia, May 29–31, 1996, M. Kh. Khankhasaev, Zh. B. Kurmanov and H. S. Plendl, eds., World Scientific, Singapore, 1997, p. 3, references therein, and following papers in these Proceedings.
- [6] C. D. Bowman, Proc. 2nd Int. Conf. on Accelerator Driven Transmutation Technology and Applications, Kalmar, Sweden, June 3-7, 1996, H. Condé, ed., Uppsala University Press, 1997, p. 11, references therein, and other papers in these Proceedings.
- [7] F. Venneri, “ATW Overview,” MIT ATW Technical Review, January 15-16, 1998 and paper in the present issue of NIM A.
- [8] H. S. Plendl, Nucl. Instr. Meth. A 414 (1998) 1, references therein, and following papers in this issue.
- [9] S. G. Mashnik, A. J. Sierk, K. A. Van Riper, and W. B. Wilson, “Production and Validation of Isotope Production Cross Section Library for Neutrons and Protons to 1.7 GeV,” Los Alamos National Laboratory Report LA-UR-98-6000 (1998); Eprint: **nucl-th/9812071**; Proc. Fourth Workshop on Simulating Accelerator Radiation Environments (SARE4), Knoxville, TN, September 13-16, 1998.
- [10] K. A. Van Riper, S. G. Mashnik, and W. B. Wilson, *Study of Isotope Production in High Power Accelerator*, (684 page detailed report with 37 tables and 264 color figures), Los Alamos National Laboratory Report LA-UR-98-5379 (1998); [hppt://t2.lanl.gov/publications/publications.html](http://t2.lanl.gov/publications/publications.html).
- [11] M. Blann, H. Gruppelar, P. Nagel, and J. Rodens, *International Code Comparison for Intermediate Energy Nuclear Data*, NEA OECD, Paris (1994); R. Michel and P. Nagel, *International Codes and Model Intercomparison for Intermediate Energy Activation Yields*, NSC/DOC(97)-1, OECD, Paris (1997); <http://www.nea.fr/html/science/pt/ieay>.
- [12] S. G. Mashnik, A. J. Sierk, O. Bersillon, and T. A. Gabriel, *Nucl. Instr. Meth.*, **A414** (1998) 68; LANL Report LA-UR-97-2905 (1997); see the detailed report on the Web at: <http://t2.lanl.gov/publications/publications.html>.
- [13] A. J. Koning, M. B. Chadwick, R. E. MacFarlane, S. G. Mashnik, and W. B. Wilson, “Neutron and Proton Transmutation/Activation Libraries Up to 150 MeV,” to be published.
- [14] Yu. E. Titarenko et al., Nucl. Instr. Meth. A 414 (1998) 73; *Proc. Second Int. Topical Meeting on Nuclear Applications of Accelerator Technology (AccApp'98)*, Gatlinburg, TN, USA, September 20-23, 1998 and references therein.
- [15] K. K. Gudima, S. G. Mashnik, and V. D. Toneev, Nucl. Phys. A 401 (1983) 329.

- [16] S. G. Mashnik, “User Manual for the Code CEM95,” JINR, Dubna (1995), OECD NEA Data Bank, Paris, France (1995); RSIC-PSR-357, Oak Ridge, 1995; <http://www.nea.fr/abs/html/iaea1247.html>.
- [17] R. E. Prael and H. Lichtenstein, “User Guide to LCS: The LAHET Code System,” LA-UR-89-3014, LANL (1989).
- [18] R. E. Prael and D. G. Madland, “LAHET Code System Modifications for *LAHET 2.8*,” LA-UR-95-3605, LANL (1996).
- [19] S. G. Mashnik and A. J. Sierk, “Improved Cascade-Exciton Model of Nuclear Reactions”, Los Alamos National Laboratory Report LA-UR-98-5999 (1998); Eprint: **nucl-th/9812069**; Proc. Fourth Workshop on Simulating Accelerator Radiation Environments (SARE4), Knoxville, TN, September 13-16, 1998.
- [20] M. Blann, Phys. Rev. C 54 (1996) 1341; M. Blann and M. B. Chadwick, Phys. Rev. C 57 (1998) 233.
- [21] M. B. Chadwick, private communication on 150-MeV n & p calculations, to be published.
- [22] D. W. Muir and A. J. Koning, Proc. Second International Conference on Accelerator-Driven Transmutation Technologies and Applications, Kalmar, Sweden, June 3-7, 1996, H. Condé, ed., Uppsala University Press, 1997, p. 469.
- [23] J.-Ch. Sublet, J. Kopecky, R. A. Forrest, and D. Nierop, “The European Activation File: EAF-97 Report file-Rev. 1,” UKAEA, Culham, Abigdon, Oxfordshire OX 14 B, United Kingdom (1997).
- [24] M. Herman, “LANL Update II of the ECNAF Neutron Activation Cross-Section Library,” Los Alamos National Laboratory Report LA-UR-96-4914 (1996).